Journal of Materials Chemistry C

ROYAL SOCIETY OF CHEMISTRY

PAPER

Check for updates

Cite this: *J. Mater. Chem. C*, 2023, **11**, 15084

View Article Online
View Journal | View Issue

Diethoxycarbonyl-BODIPYs as heavy-atom-free photosensitizers for holographic recording in cellulose acetate photopolymer†

Aimee Sheehan, [a] Tatsiana Mikulchyk, [b] Catherine S. P. De Castro, [c] Safakath Karuthedath, [c] Wejdan Althobaiti, [c] Metodej Dvoracek, [a] Sabad-e-Gul, [b] Hugh J. Byrne, [d] Frédéric Laquai, [c] Izabela Naydenova [be] and Mikhail A. Filatov *[a]

A series of new heavy-atom-free photosensitizers based on the 2,6-diethoxycarbonyl-BODIPY scaffold was designed and applied for holographic recording in a photopolymerizable material. Photoinduced electron transfer between the BODIPY and *meso*-aryl subunits, followed by the formation of BODIPY triplet excited states *via* spin−orbit charge transfer intersystem crossing (SOCT-ISC) was studied by steady-state and ultrafast pump−probe transient optical spectroscopy. Highly efficient photosensitization was observed for dyads bearing pyrene and anthracene substituents, which exhibited singlet oxygen generation quantum yields (Φ_Δ) of up to 94%. Charge transfer and SOCT-ISC were observed in non-polar solvent (toluene) due to the increased electron accepting ability of the diethoxycarbonyl-BODIPY. In combination with *N*-phenylglycine (NPG) as a co-initiator, new BODIPYs initiate a free-radical polymerization of acrylamide monomers under 532 nm irradiation that was used for creation of volume phase transmission gratings in a photopolymerizable material based on cellulose acetate and polyethylene glycol (CA−PEG). As a result of holographic recording, diffractive structures with diffraction efficiency of up to 56% were obtained for CA−PEG layers sensitized with BODIPY-pyrene dyad as compared to a reference heavy-atom-containing diiodo-BODIPY dye (27%). The developed materials showed refractive index modulation of up to 2.3 × 10^{-3}, which demonstrates the potential of diethoxycarbonyl-BODIPYs photosensitizers for holographic recording applications.

[a] *School of Chemical and Biopharmaceutical Sciences, Technological University Dublin, City Campus, Grangegorman, Dublin 7, Ireland.*
E-mail: mikhail.filatov@tudublin.ie
[b] *Centre for Industrial & Engineering Optics, Technological University Dublin, D07 ADY7 Dublin, Ireland*
[c] *King Abdullah University of Science and Technology (KAUST), KAUST Solar Center (KSC), Physical Sciences and Engineering Division (PSE), Material Science and Engineering Program (MSE), Thuwal 23955-6900, Kingdom of Saudi Arabia*
[d] *FOCAS Research Institute, Technological University Dublin, City Campus, Camden Row, Dublin 8, D08 CKP1 Dublin, Ireland*
[e] *School of Physics, Clinical & Optometric Sciences, Technological University Dublin, D07 ADY7 Dublin, Ireland*
† Electronic supplementary information (ESI) available. See DOI: https://doi.org/10.1039/d3tc02640j

Introduction

Photopolymerization is nowadays used in a number of technologies and its application scope is constantly expanding. In particular, UV curing is a very popular technique used for the assembly of a variety of products and materials. However, UV light has low penetration depth, high energy consumption, and potential to damage materials from overexposure.[1] Carrying out photopolymerization using safer and lower energy (*i.e.* visible light) photons has significant advantages as visible light has greater penetration power which is more suitable for highly pigmented polymers.[2] Many organic and inorganic compounds are also sensitive to UV irradiation, and thus curing with visible light avoids the occurrence of unwanted side reactions arising from degradation of the materials.[3]

The development of efficient visible light driven photoinitiating systems is the focus of intense research effort. Such systems are usually based on a combination of organic dyes known as photosensitizers (PSs) and various additives (*e.g.*, iodonium salt, amines, silane, *etc.*) which act as co-initiators.[4] A photosensitizer component undergoes intersystem crossing (ISC) and forms long-living triplet excited states which are able to initiate chemical transformation leading to free radical formation and thus cause polymerization. ISC is a spin-forbidden process and so chemical structures of potential PSs must be rationally designed to enhance triplet state yields (Φ_T) and lifetimes (τ_T).[5] ISC can be promoted in organic dyes by the

introduction of heavy atoms, such as iodine and bromine, or transition metals which are known to enhance spin–orbit coupling.[6] However, this approach has significant drawbacks such as higher costs and unwanted side effects, including negative environmental impact, increased toxicity and shortened triplet state lifetimes.[7]

Spin–orbit charge transfer intersystem crossing (SOCT-ISC) represents an attractive alternative approach for generating long living triplet excited states in heavy-atom-free molecules. This ISC mechanism has attracted much attention in recent years and corresponding dyes found some unique niches in applications such as photodynamic therapy (PDT)[8] and triplet–triplet annihilation upconversion (TTA-UC).[9] Boron dipyrromethene (BODIPY) dyes[10] are so-far the most well-studied class of compounds undergoing SOCT-ISC. Due to their excellent spectroscopic characteristics and convenient synthesis, introducing substituents in almost any position in the core structure is possible thus allowing to tune molecular geometries and excited state energies, and as a result the SOCT-ISC in BODIPYs can be effectively optimized.[11]

Heavy-atom-free BODIPY photosensitizers were recently demonstrated by us as efficient photoinitiators for free-radical polymerization of acrylate monomers.[12] Notably these PSs showed comparable or even higher photopolymerization rates than the reference heavy-atom-containing diiodo-substituted BODIPY which forms triplet excited states due to enhanced spin–orbit coupling. However, developing BODIPY-based photoinitiating systems that efficiently initiate the free radical polymerization for a wide range of monomers under mild irradiation conditions (low light intensity and under air) is still a challenge.[13] One of the complications is a strong dependence of triplet state yields on solvent polarity, which is a known characteristic of SOCT-ISC. Recently Uddin *et al.* demonstrated this by using several BODIPY donor–acceptor dyads as photoinitiators for the polymerization of monomers of varying polarity.[14] A general decrease in polymerization rate was observed as monomer polarity increased, however the magnitude of the polarity effect varied between dyes. This was attributed to differences in the CT state stabilization pathways of the BODIPYs. Dyes capable of undergoing efficient SOCT-ISC in low polarity solvents are beneficial, because monomers and formulations used for polymerization are relatively non-polar. The polarity of the matrix also decreases as the polymerization process occurs due to the conversion of more polar carbon–carbon double bonds into less polar single bonds.[15]

Efficient SOCT-ISC in low and moderate polarity solvents can be achieved by introducing electron-accepting substituents in the dipyrromethene core.[11] However, this often leads to a decrease in triplet state yields due to enhancement of ground state recombination rate ($CT \rightarrow S_0$), due to stabilization of the CT state by electron-withdrawing groups and narrowing $CT–S_0$ energy gap (Fig. 1(a)).[16] It is also difficult to design PSs efficiently operating in a broad range of polarities or predict the triplet state yield for different solvents based on the structure. Although recent efforts have shown that it is possible to accurately predict singlet oxygen generation quantum yields
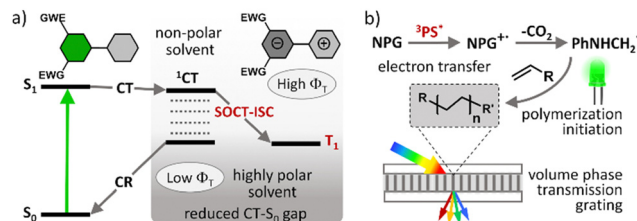

Fig. 1 (a) Qualitative Jablonski diagrams depicting photophysical mechanisms of triplet state formation *via* SOCT-ISC in a donor–acceptor dyad. (b) Schematic representation of volume transmission gratings formation as a result of a spatially controlled photopolymerization.

(Φ_Δ) for BODIPYs by using quantitative structure–property relationship (QSPR) and machine-learning techniques,[17] such computational methods are still being optimized.

In this work we investigated new BODIPY dyes containing electron-withdrawing ethoxycarbonyl substituents in positions 2 and 6, which promote electron transfer and allow for efficient SOCT-ISC in both polar and non-polar solvents, such as toluene. Different electron donor substituents, such as anthracenyl, pyrenyl and methoxyphenyl groups, were employed in the *meso* position to modulate the donor–acceptor capability of the BODIPYs and in turn optimize the formation of long-living triplet excited states *via* SOCT-ISC. Highly efficient charge transfer and triplet states formation in a non-polar solvent was confirmed by short and long delay transient absorption measurements and singlet oxygen ($^1O_2$) quantum yield (Φ_Δ) measurements which showed values of up to 94% in toluene. Further, the photosensitizing ability of diethoxycarbonyl-BODIPY dyes was evaluated by employing them as photoinitiators in free-radical polymerization of acrylamide monomers and recording of holographic structures.

The photopolymer used in this work is based on a cellulose acetate–polyethylene glycol (CA–PEG, Fig. 2) matrix, containing acrylamide as a monomer and *N,N*-methylenebisacrylamide as a cross-linker, which provides increased stability of the hologram in water.[18] Diethoxycarbonyl-BODIPYs were employed as photosensitizers in a two-component photoinitiating system containing *N*-phenylglycine (NPG)[19] as a co-initiator. NPG was chosen as a co-initiator as its efficiency for the free-radical polymerization has been previously demonstrated in a photosensitive resin for 3D printing[20] and in holographic recording materials.[21,22] NPG was shown to react with triplet excited states of photosensitizers, undergoing electron transfer and forming corresponding radical cation (NPG•+)[23] which further undergoes deprotonation/decarboxylation to give anilino-methyl radical (PhNHCH$_2$•) that initiates polymerization of methacrylate and acrylamide monomers (Fig. 1(b)).[24] Cellulose acetate was selected as a binder for the following key reasons: (1) the layers produced in this binder are not sensitive to humidity and the optical devices recorded in the layers have unchanged diffraction efficiency after being immersed in water;[18] (2) the obtained solid layers are of high optical quality and show very low scattering;[18] (3) it is possible to control the porosity of the binder by varying the PEG concentration, which is needed for the development of holographic sensors.[18]
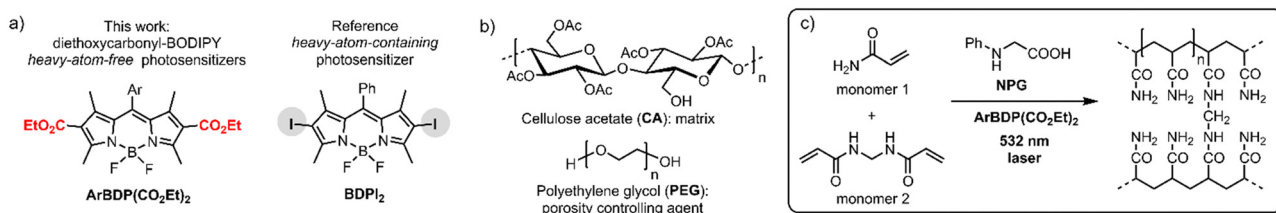
This journal is © The Royal Society of Chemistry 2023

J. Mater. Chem. C, 2023, **11**, 15084–15096 | **15085**

Fig. 2 Chemical components of the studied photopolymer: structures of (a) dyes used as photoinitiators, (b) polymeric matrix – cellulose acetate (CA) and polyethylene glycol (PEG). (c) Photopolymerization of acrylamide (monomer 1) and *N,N*-methylenebisacrylamide (monomer 2, crosslinker) initiated by NPG–BODIPY system under 532 nm excitation.

Holographic recording in photopolymers uses the wave interference of light to create the refractive index modulation and, as a result, form a diffraction grating.[25] In this work, transmission gratings with the spatial frequency of 800 lines per mm were recorded in the photopolymer layers sensitized with BODIPYs. Performance of these new photosensitizers was studied through real-time recording of diffraction efficiency growth, which was compared to the reference heavy-atom-containing dye, *meso*-phenyl-2,6-diiodoBODIPY (**BDPI₂**). The obtained results prove that ethoxycarbonyl BODIPYs are efficient photosensitizers for polymerization of acrylate monomers in the CA–PEG matrix. The resulting photopolymers displayed higher exposure sensitivity achieving diffraction efficiency of up to 56%, compared to 27% for **BDPI₂**. These results expand the arsenal of sustainable, environment-friendly, stable and highly efficient photopolymerizable materials for holographic recording under green light excitation.

Results and discussion

### Synthesis of diethoxycarbonyl-BODIPY dyads

To systematically investigate the optical characteristics of diethoxycarbonyl-BODIPY and optimize the triplets formation *via* SOCT-ISC, a series of compounds containing different aromatic groups were synthesized. Corresponding precursor, 3-ethoxycarbonyl-2,4-dimethylpyrrole (**P3**) was prepared using a two-step procedure: commercially available diethyl-2,4-dimethylpyrrole-3,5-dicarboxylate (**P1**) was hydrolysed into a corresponding carboxylic acid (**P2**) (Scheme 1(a)), followed by

a decarboxylation at 210 °C to produce pyrrole **P3** in high overall yield.[26]

meso-Unsubstituted 2,6-diethoxycarbonyl-BODIPY (**BDP 1**) was one of the first BODIPYs described by Treibs and Kreuzer in 1968,[27] and since then has been used as a precursor for syntheses of ring-fused dyes.[28] It was prepared in a three-step reaction (Scheme 1(a)): pyrrole **P3** was reacted with dimethoxymethane to give corresponding dipyrromethane which was further oxidised with 2,3-dichloro-5,6-dicyano-1,4-benzoquinone (DDQ), followed by the insertion of boron, using boron trifluoride diethyl etherate (BF₃·Et₂O) in the presence of *N,N*-diisopropylethylamine (DIPEA) to give **BDP 1** in 29% overall yield.

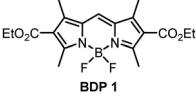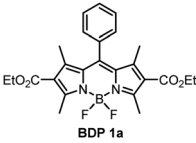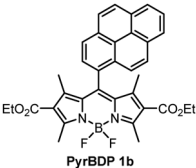### Steady-state absorption and photoluminescence emission properties of the dyads
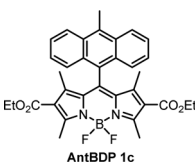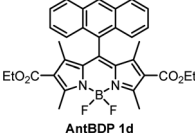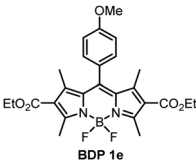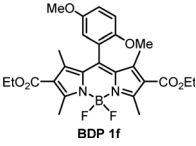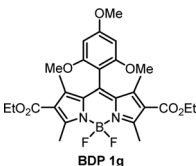
The absorption and fluorescence emission parameters of diethoxycarbonyl BODIPYs in a range of solvents are given in Table 1. Reference compounds **BDP 1** and **BDP 1a** which lack electron donor groups and thus do not undergo intramolecular charge transfer showed optical properties typical for alkyl-substituted BODIPYs, *i.e.* narrow absorption and emission bands, high fluorescence quantum yields (Φ_{em}) both in polar and non-polar solvents. For *meso*-phenyl **BDP 1a** (Fig. 3(a)), position of the absorption and emission bands are nearly identical to the parent 1,3,5,7-tetramethyl BODIPY (λ_{abs} = 498 nm, λ_{em} = 508 nm in methanol),[29] indicating that introduction of electron-deficient ethoxycarbonyl in the 2,6 positions has no major effect on optical characteristics. This is in line
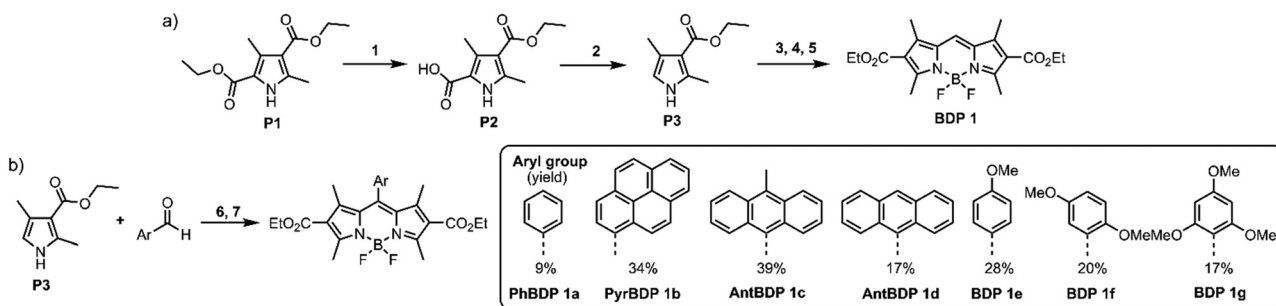
Scheme 1 (a) Synthesis of pyrrole precursor and *meso*-unsubstituted diester BODIPY. Reagents and conditions: (1) KOH, ethanol–H₂O, reflux (80%); (2) N₂, 1 h, 210 °C (79%); (3) dimethoxymethane, *p*-toluenesulfonic acid, N₂, acetic acid, 18 h, r.t.; (4) DDQ, DCM, 20 min, r.t.; (5) BF₃·Et₂O, DIPEA, N₂, DCM (anh.), 2 h, r.t. (29% over steps 3–5). (b) Synthesis of *meso*-aryl diethoxycarbonyl-BODIPYs. Reagents and conditions: (6) (i) trifluoroacetic acid, N₂, DCM (anh.), 12 h, r.t.; (ii) DDQ, DCM, 10 min, r.t.; (7) BF₃·Et₂O, DIPEA, N₂, DCM (anh.), 2 h, r.t. (9–39% over steps 6–7).

Table 1 Steady-state spectroscopic data for diethoxycarbonyl-BODIPY compounds in various solvents

Compound	Solvent[a]	λ_{abs}[b] (nm)	λ_{em}[cd] (nm)	Φ_{em}[de]	Compound	Solvent	λ_{abs} (nm)	λ_{em} (nm)	Φ_{em}
BDP 1	ACN	496	505	0.958	BDP 1a	CAN	497	507	0.413
	EtOH	497	506	0.995		EtOH	497	508	0.537
	THF	500	509	0.977		THF	499	511	0.668
	DCM	502	511	0.919		DCM	500	511	0.555
	TOL	507	517	0.966		TOL	503	516	0.646
	HEX	504	511	0.960		HEX	501	512	0.725
PyrBDP 1b	CAN	500	517, 704	0.002	AntBDP 1c	ACN	501	513	0.040
	EtOH	497	510, 673	0.015		EtOH	501	514	0.063
	THF	503	516, 634	0.002		THF	503	516	0.074
	DCM	504	520, 641	0.003		DCM	504	516	0.064
	TOL	507	521	0.220		TOL	507	520	0.055
	HEX	503	514	0.773		HEX	504	515	0.225
AntBDP 1d	ACN	500	522	0.028	BDP 1e	ACN	497	509	0.374
	EtOH	502	523	0.026		EtOH	498	510	0.545
	THF	504	525	0.041		THF	500	513	0.547
	DCM	505	519	0.008		DCM	500	513	0.630
	TOL	508	521	0.006		TOL	503	518	0.603
	HEX	505	516	0.382		HEX	501	513	0.380
BDP 1f	ACN	499	507	<0.001	BDP 1g	ACN	501	514	0.002
	EtOH	500	518	<0.001		EtOH	503	515	0.011
	THF	503	513	0.001		THF	505	517	0.212
	DCM	504	515	0.002		DCM	506	517	0.301
	TOL	507	522	0.158		TOL	509	521	0.941
	HEX	504	515	0.996		HEX	506	516	0.764

[a] Concentration of the samples: 5×10^{-6} M. HEX – hexane, TOL – toluene, THF – tetrahydrofuran, DCM – dichloromethane, EtOH – ethanol, ACN – acetonitrile. [b] Absorption maxima corresponding to BODIPY chromophore. [c] Fluorescence was recorded by exciting the samples at the vibrational shoulder of the BODIPY absorption. Excitation wavelength: 470 nm. [d] The fluorescence quantum yields were measured using Rhodamine 6G as a standard ($\Phi_{em} = 0.95$ in EtOH).[36] [e] Fluorescence quantum yield value representing the integral emission coming from locally excited (LE) and charge-transfer (CT) excited states.

with the work of Gabe *et al.* describing the compound **BPD 1a** and its analogue, *meso*-phenyl-2,6-diethyl-1,3,5,7-tetramethyl BODIPY.[30] While the absorption and emission maxima of the BODIPY are not affected by ethoxycarbonyl groups, the addition of electron-rich ethyl groups to the 2,6-positions causes a strong bathochromic shift (λ_{abs} = 520 nm, λ_{em} = 534 nm, Fig. 3(a)) due to increasing HOMO energy level of the BODIPY fluorophore.[31]

The optical properties of **BPD 1a**, pyrene and anthracene dyads **1b** and **1c**, respectively, are presented in Fig. 3 and summarized in Table 1. The absorption spectra show transitions associated with the two subunits, indicating weak coupling of the chromophores in the ground state. Upon changing the solvent polarity, the shape and maxima of the absorption undergo little change (Fig. S10, ESI†), but the emission properties are greatly affected. Fig. 3(b) shows the emission spectra of pyrene dyad **1b** in different solvents. In THF the local exciton (LE) peak appears at 516 nm, and is accompanied by broad band centred at 634 nm. This second signal can also be seen in the emission spectrum in EtOH, further red-shifted to 672 nm. These bands are not seen in the emission spectra of **PyrBDP 1b** in toluene or hexane, indicating that the energy of the corresponding excited state strongly depends on the solvent polarity. The appearance of these broader signals is accompanied by a remarkable drop in emission intensity and quantum yield to

0.002 in THF and 0.015 in EtOH. It should be noted that the observed photoluminescence emission is concentration dependent: bathochromic shift of up to 15 nm was observed both for reference BODIPY and for the studied donor acceptor dyads when increasing the dye concentration (Fig. S11, ESI†); similar behaviour was previously observed for BODIPYs forming J-aggregates.[32]

In line with previous reports,[33] weak emission above 600 nm can be attributed to a charge transfer state between the pyrene and BODIPY subunits. The reported reduction potential E_{A/A^-} for the diethoxycarbonyl-BODIPY group is −0.87 eV (MeCN/SCE), which is +0.32 eV more positive than the value reported for the reference 1,3,5,7-tetramethyl BODIPY that has hydrogen atoms at the 2,6-positions.[34] This makes diethoxycarbonyl-BODIPY chromophore more susceptible to reduction and facilitates charge transfer. The oxidation potential (E_{D/D^+}) of pyrene group in acetonitrile is 1.16 eV,[35] making the electron transfer to the BODIPY subunit thermodynamically favourable. In the dyad molecule, pyrene acts as an electron donor and the BODIPY as an acceptor, allowing a dipolar CT state to form. The emission observed for pyrene dyad **1b** in THF and ethanol (Fig. 3(b)) can be interpreted as a combination of fluorescence from the LE and CT state. When compared to the previously reported 1,3,5,7-tetramethyl BODIPY-pyrene dyad without
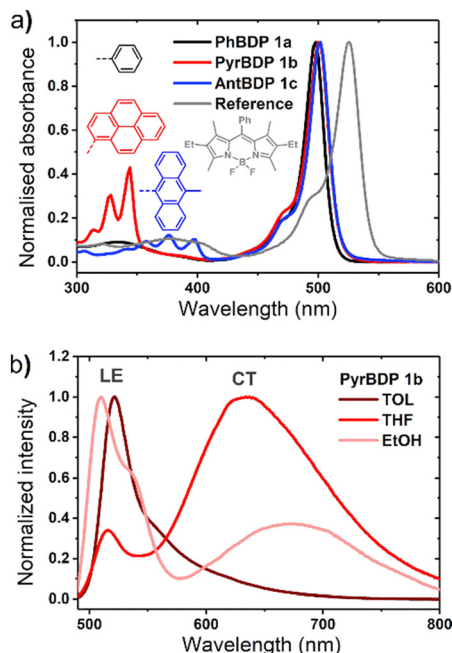
This journal is © The Royal Society of Chemistry 2023

J. Mater. Chem. C, 2023, **11**, 15084–15096 | **15087**

Fig. 3 (a) Normalized absorption of **PhBDP 1a, PyrBDP 1b, AntBDP 1c** and a reference BODIPY compound in ethanol. (b) Normalized photoluminescence emission spectra of pyrene dyad **1b** in a range of solvents (λ_{exc} = 470 nm). Concentration of samples: 5×10^{-6} M. TOL – toluene, THF – tetrahydrofuran, EtOH – ethanol.

ethoxycarbonyl groups, which showed only moderate charge transfer efficiency in polar solvents;[33a] it can be concluded that the addition of these substituents has promoted intramolecular charge transfer efficiency in the dyad.

The emission of **AntBDP 1c** in toluene shows a similar CT fluorescence at 625 nm (Fig. S10, ESI†). The Φ_{em} values decreases considerably from 0.225 for nonpolar hexane to 0.04 in ACN. This can be rationalized by taking into account lower oxidation potential of 9-methylanthracene fragment (1.04 eV),[16] compared to pyrene (1.16 eV), which increases the driving force of the electron transfer process making it feasible in non-polar toluene. Previously reported BODIPY-anthracene dyads, which lack electron-withdrawing groups in the 2,6 positions, undergo charge transfer only in polar solvents such as ACN and DCM.[37]

For compounds **BDP 1e–g** containing different number of methoxy substituents in the *meso*-phenyl group, the absorption spectra show strong $S_0 \rightarrow S_1$ transitions at around 500 nm, with slight red shifts of 6–9 nm as solvent polarity increases. There is also $S_0 \rightarrow S_2$ transitions at $\approx$350 nm from the phenyl subunit, indicating that the electronic coupling with the BODIPY core in the ground state is weak. Upon changing the solvent polarity, the shape and maxima of the absorption and emission bands of **BDP 1e–g** undergo little change. However, changes can be seen in the emission quantum yields (Φ_{em}), particularly for **BDP 1f** where Φ_{em} varies from <0.001 in EtOH up to 1 in hexane. As the dyads have the same ethoxycarbonyl-substituted core, the difference in emission yields between **BDP 1e, 1f** and **1g** must

be due to the changes in methoxy-substituents in the *meso*-phenyl group.

As is seen from Table 1, the fluorescence quantum yields values for **BDP 1e** in different solvents are very similar to those of *meso*-phenylBODIPY **BDP 1a** and, in general, are not affected by solvent polarity. For **BDP 1f** and **1g**, fluorescence is strongly quenched in polar solvents, indicating efficient charge transfer. This difference can also be rationalized taking into account oxidation potentials (E_{ox}) of the *meso*-methoxybenzene substituents, which are: 1.77 eV for anisole (**BDP 1e**), 1.55 eV for 1,3-dimethoxybenze (**BDP 1f**) and 1.54 eV for 1,3,5-trimethoxybenzene (**BDP 1g**).[38] Increasing the number of methoxy-substituents on the phenyl ring leads to lowering the E_{ox} and, consequently, increases the driving force of electron transfer from these subunits to the BODIPY core. This is in line with previous reports on BODIPYs bearing methoxy-, dimethoxy- and trimethoxyphenyl groups in the *meso*-position.[17] In addition, the presence of methoxy groups in the *ortho* position could potentially hinder the rotation of the *meso*-aryl donor, making the geometry of the dyad orthogonal and in turn promoting SOCT-ISC.[39]

To assess the efficiency of triplet state formation in different solvents, the singlet oxygen quantum yields were determined through a chemical-trapping method, employing 1,9-dimethylanthracene (DMA) as a $^1O_2$ sensor. DMA selectively reacts with singlet oxygen giving a corresponding endoperoxide.[40] For the measurements, solutions of DMA in air-saturated solvent containing corresponding BODIPY were irradiated with light at 514 nm with a constant 12 mW cm^{-2} power for periods of 30–120 s, after which the absorption spectra were recorded. The BODIPY absorption shows no change during irradiation, while the DMA absorption decreases linearly over time (Fig. 4, inset). This change is plotted, and the slope is then used to determine Φ_Δ as compared to the reference photosensitizer as described in Section S6 of the ESI.†

The results from the singlet oxygen quantum yield measurements on the diethoxycarbonyl-BODIPYs can be seen in Table 2 below. The parent compounds **BPD 1** and **BPD 1a** have very low Φ_Δ in each solvent, ranging from 0.004–0.027. This correlates
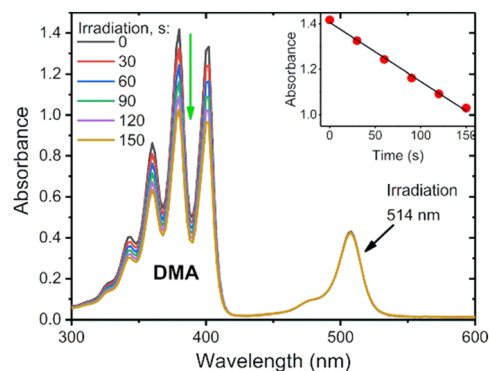

Fig. 4 Photosensitized oxidation of 1,9-dimethylanthracene in the presence of **AntBDP 1c** in air saturated toluene solution irradiated with 514 nm laser (12 mW cm^{-2}). Inset: Change of absorbance at 376 nm with time.

15088 | *J. Mater. Chem. C*, 2023, **11**, 15084–15096

This journal is © The Royal Society of Chemistry 2023

Table 2 Quantum yields of singlet oxygen photosensitization by diethoxycarbonyl-BODIPY compounds in various solvents[a]

Compound	EtOH	ACN	THF	TOL
BDP 1	0.011	0.016	0.025	0.027
BDP 1a	0.006	0.005	0.004	0.005
PyrBDP 1b	0.294	0.117	0.548	0.504
AntBDP 1c	0.211	0.075	0.511	0.941
AntBDP 1d	0.467	0.290	0.337	0.515
BDP 1e	0.004	0.011	0.051	0.007
BDP 1f	0.015	0.005	0.045	0.264
BDP 1g	0.146	0.141	0.221	0.011

[a] Quantum yields were measured using 1,9-dimethylanthracene as a $^1O_2$ trap and 2,6-diiodo-8-phenylBODIPY as a reference photosensitizer (0.85 in toluene).[41]

with their strong emissive properties discussed previously. Pyrene dyad **1b** shows moderate variations of Φ_Δ in different solvents, with its highest result of 0.548 obtained in toluene, overall, the second highest yield obtained from these measurements.

While the Φ_Δ varies greatly between solvents for some dyads, unlike Φ_{em}, there appears to be no direct correlation between $^1O_2$ quantum yield and solvent polarity. This is evident for **AntBDP 1c**, which has the highest yield overall of 0.961 in nonpolar toluene, and a much lower yield of 0.075 in more polar

acetonitrile. Compound **AntBDP 1d**, which differs in structure from **AntBDP 1c** only by the absence of a methyl group in position 9 of the anthracene subunit, does not have the same high yield in toluene. Φ_Δ values of **AntBDP 1d** have less variation than those of **AntBDP 1c**, and its highest result of 0.515 is also recorded in toluene. Reference BODIPY-pyrene and anthracene dyads which lack ethoxycarbonyl groups in positions 2,6 of the BODIPY scaffold are summarized in Table S1 (ESI†). For 8-pyrenyl-1,3,5,7-tetramethylBODIPY, Φ_Δ value of 0.088 was recorded in toluene which is consistent with strong fluorescence ($\Phi_F = 0.926$)[33a] in this solvent and thus can be explained by inefficient charge transfer in non-polar solvent environment.

The methoxybenzene-substituted dyads **1e–g** all have relatively low Φ_Δ values in all solvents, the highest being recorded for **BDP 1f** in toluene with a yield of 0.264. **BDP 1e** is the least efficient $^1O_2$ generator of these three dyads, with a maximum value of 0.051 in THF. **BDP 1e** also has very low Φ_{em} as stated previously, due to inefficient charge transfer.

Femto- and nanosecond pump–probe transient absorption spectroscopy

To reveal the photoexcited state dynamics of pyrene and anthracene dyads **1b** and **1c** dyads, respectively, transient
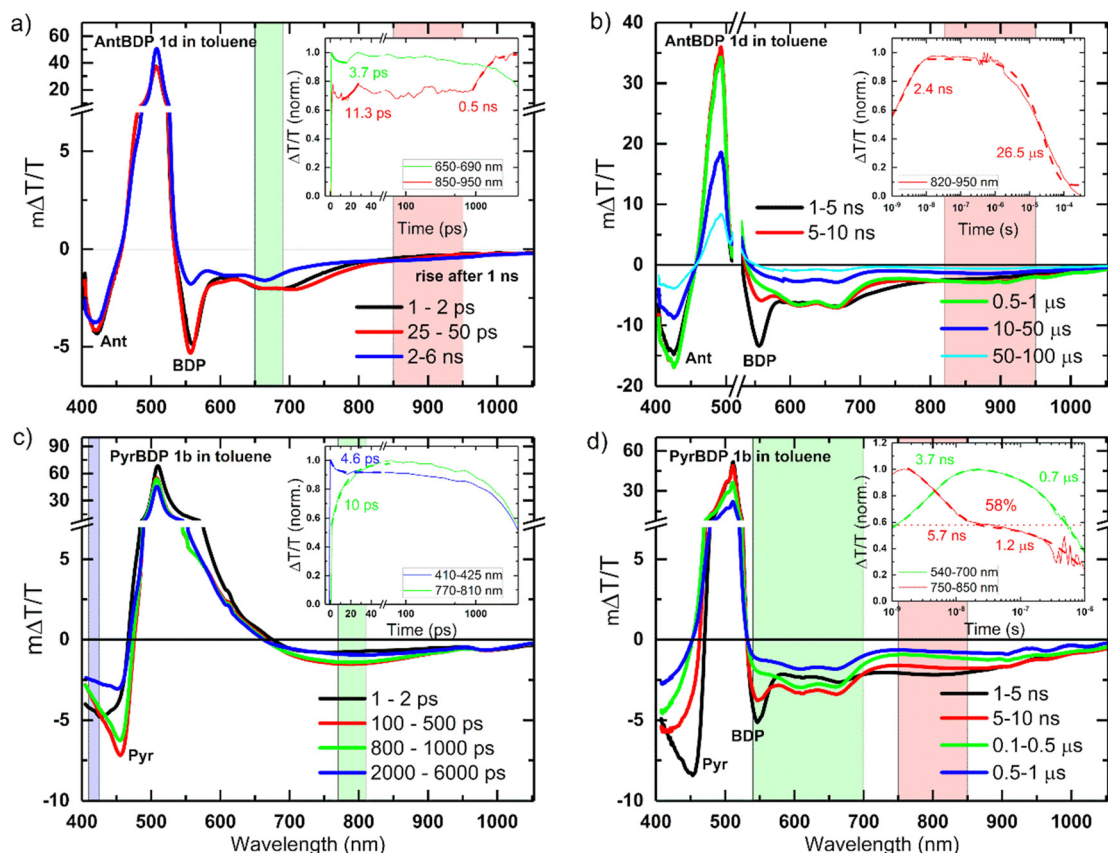
Fig. 5 ps–ns (a) and (c) and ns–μs (b) and (d) TA spectra with kinetics (as green, red and blue insets) of the selected spectral region (shadowed in corresponding green, red and blue areas) of pyrene and anthracene dyads **PyrBDP 1b** and **AntBDP 1c** in toluene after excitation with 505 nm and 532 nm laser pulses, respectively, under inert atmosphere. Pyr, Ant and BDP stand for pyrene, anthracene and BODIPY, respectively. The spectra are labelled with these where their signatures are clearly seen. When the kinetics were fitted, the fits were shown in insets together with their respective rate constants.

This journal is © The Royal Society of Chemistry 2023

J. Mater. Chem. C, 2023, **11**, 15084–15096 | **15089**

absorption (TA) spectroscopy was employed. Fig. 5 shows the picosecond–nanosecond (ps–ns) and nanosecond–microsecond (ns–μs) TA spectra and kinetics of selected spectral regions shadowed (as insets) of **1c** (a and b) and **1b** (c and d) in toluene after photoexcitation at 505 nm (ps–ns TA) and 532 nm (ns–μs TA), respectively. The negative $\Delta T/T$ signals represent photoinduced absorption (PA), whereas the positive $\Delta T/T$ signals represent photo-bleaching (PB). In Fig. 5, we can attribute the band centred at 500–510 nm to the PB of BODIPY (BDP), clearly seen in Fig. 5 panels a, b and d.[37] Stimulated emission can be observed in the PB broadening ∼550 nm, for **PyrBDP 1b** in toluene (see Fig. S15, ESI†). The PA region of **AntBPD 1c** at ∼420 nm corresponds to the tail of the anthracene exciton-induced absorption (Ant), observable in both toluene (Fig. 5(a) and (b)) and acetonitrile (Fig. S16, ESI†).[42]

The same can be seen for **PyrBDP 1b** in acetonitrile with a clear pyrene exciton-induced absorption (Pyr) signature at ∼460 nm readily visible at 1–2 ps (Fig. S16b, ESI†), but visible only at later times (100–500 ps) in toluene (Fig. 5(c)).[43]

The BODIPY exciton-induced absorption (BDP) can be readily (1–2 ps) seen at around 549–558 nm and 547–556 nm, for **AntBDP 1c** and **PyrBDP 1b**, respectively, but only later for dyad **PyrBDP 1b** in toluene (1–5 ns) due to the overlap with its stimulated emission (Fig. 5(a) and (c)).

The PA regions centred at ∼420 nm and ∼800 nm (clearer in Fig. 5(d) for compound **PyrBDP 1b** in toluene) showed a spectral evolution with time consistent with the formation of charge-transfer (CT) states, as described in previous work.[12] The negligible temporal evolution of the PB band in toluene (except for **1b** and **1c** at later times) is due to both photoexcited singlet and CT states exhibiting the same photobleaching, and the population of CT states from singlet excited states. The kinetics of the band at 550–570 nm exhibited a clear decay until 10 ps, but no further changes were observed after that up to 500 ps, while the 770–870 nm band exhibited a clear rise due to the generation of CT states (inset Fig. 5(c)).

An exponential fit to the dynamics yielded an inverse rate constant of 4–5 ps for the singlet exciton decay and 10–11 ps for the CT state generation probed at 550–570 nm and 770–870 nm in toluene, respectively (Fig. 5(c)). The ps–ns TA spectra of both dyads **1c** and **1b** in acetonitrile showed different spectral shapes and evolution (Fig. S16, ESI†) where the PB band in acetonitrile showed an immediate decay, compared to **AntBDP 1c** in toluene. This is supported by the fast decay of the CT states (band centered at 630 nm). Table S2 (ESI†) summarizes the inverse generation rates of CT states in both toluene and acetonitrile.

The spectral shape and evolution are different for **PyrBDP 1b** in acetonitrile compared to toluene (Fig. S16, ESI† and Fig. 5, respectively). In acetonitrile, both molecules showed early time (after 10 ps), and faster decay of the CT states compared to the toluene solutions. Dyads **1b** and **1c** showed a clear difference in the spectra and dynamics of the excited states. In **PyrBDP 1b** (Fig. 5(d)), the CT state peaked at around 800 nm and decayed within ∼10 ns, causing the emergence of two new long-lived bands at 600 nm and 670 nm. We assigned these bands to the

BODIPY triplet state based on previous reports.[12] An exponential fit to the kinetics shown in the inset of Fig. 5(d) yielded an inverse rate constant of 5.7 ns for the triplet generation and 0.7–1.2 μs for the triplet decay for **PyrBDP 1c** much longer than that observed for **AntBDP 1b** (26.5 μs), in toluene, which are significantly shorter than those obtained for both dyads in acetonitrile (∼65 μs, Fig. S16b and d, ESI†). For **AntBDP 1c** in toluene, we estimated a triplet yield of 58% (see the horizontal dashed line in the inset Fig. 5(d)), assuming both triplet and singlet states exhibit the same absorption cross-section as reported in previous works[9a,12] which agrees with the one measured by relative actinometry (56–73%) using an optically matched (at pump wavelength) Rose Bengal solution in methanol as ref. 44, see Fig. S14 and Table S2 in the ESI.† A similar analysis was done for the remaining materials and solvents combination, see Fig. S16 and Table S2 (ESI†).

Holographic recording of volume transmission gratings

During holographic recording photopolymerizable materials experience spatially varying change of the refractive index due to change in molar refractivity and local density caused by illumination with spatially varying light intensity. Such materials found use in a wide variety of technologies, e.g. data transfer[45] and storage,[25,46] holographic solar concentrators,[47] augmented and virtual reality displays.[48] The key component of such materials is a photoinitiating system that triggers polymerization in the illuminated areas leading to the refractive index modulation and, as a result, formation of the diffraction grating. The holographic recording capability (sensitivity and dynamic range) of photopolymerizable materials depends on the photoinitiating system efficiency which is determined by its light absorption properties, initiating radicals quantum yield and radicals reactivity.[49,50] Appropriate choice of the photoinitiator component is critical for the performance of photopolymerizable materials in holographic recording applications and the development of such systems is a subject of intense research. Recently, Zheng et al. have demonstrated that the use of two-component photoinitiating system Irgacue® 784 – Rose Bengal improves the stability of the grating in the epoxy resin/acrylate-based photopolymer.[51] Rolle et al. have reported a three-component system based on Safranine O dye, an electron acceptor (triazine), and an electron donor (borate salt), which generates up to two initiating radicals from one photon absorption and allows for single pulsed holographic recording in polyurethane/acrylate-based photopolymers.[52] Tomita et al. have reported a novel three-component PS consisting of cyanine dye, triazine compound and borate salt for efficient radical generation in photopolymerizable nanoparticle-polymer materials dispersed with hyperbranched polymer.[53] These developments highlight the importance of the photoinitiating system choice to achieve the full technological potential of the holographic recording material in a specific application.

In this work, holographic recording in cellulose acetate-PEG layers was employed to study the performance of novel diethoxycarbonyl-BODIPY – NPG photoinitiating system for free radical photopolymerization of acrylamide monomers under

15090 | *J. Mater. Chem. C*, 2023, **11**, 15084–15096

This journal is © The Royal Society of Chemistry 2023

illumination with 532 nm light. Due to their high triplet state yields, BODIPY-pyrene and BODIPY-anthracene dyads **PyrBDP 1b** and **AntBDP 1d**, respectively, were investigated. Although *meso*-9-methylanthracene dyad **AntBDP 1c** showed even higher triplet state yield, it can undergo cycloaddition reaction with singlet oxygen similarly to previously reported BODIPY-anthracene dyads.[37a] Dyad **AntBDP 1d** was used for photopolymerization instead, due to low reactivity of the anthracene group towards singlet oxygen as compared to 9-methylanthracene.[54]

Performance of the novel dyes is compared with reference dyes, namely, *meso*-phenylBODIPY **BDP 1a** and 2,6-diiodoBODIPY (**BDPI₂**). It is assumed that the binder polymer matrix (CA–PEG) is not reactive and is not involved in the photopolymerization process of acrylamide monomers that are evenly dispersed in the volume. CA–PEG layers containing monomers and photoinitiating system components have been prepared using a modified literature procedure,[18] as described in detail in Section S9.1 of the ESI.† The absorption spectra of the resulting materials showed characteristic BODIPY absorption bands at 503–534 nm (Fig. 6(a)). For the recording, layers with 75–105 μm thickness were obtained through a drop-casting method followed by drying under a glass dish to slow solvent evaporation, as described in the ESI.† This was in order to achieve clear, even layers across the substrate as it was observed that allowing rapid drying led to opaque, irregular layers. Dry layers showed low light scattering as seen from a clear image observed through the sample in Fig. 6(b). This allowed for a reduction in losses due to scattering of light during holographic recording and achieving high diffraction efficiency of the grating.

The polymerization of acrylamide and *N,N′*-methylenebisacrylamide in the CA–PEG materials under 532 nm excitation was confirmed by using Raman microspectroscopy, which has been previously used to study photopolymerization of these monomers.[55] The reaction progress was monitored by changes in the characteristic vibrational peaks at 1600 cm⁻¹ and 1623 cm⁻¹, which correspond to the C═C double bonds of acrylamide and methylenebisacrylamide, respectively. The spectrometer is equipped with both 785 nm and 532 nm lasers as options for Raman source (Fig. S18, ESI†), and therefore the

532 nm laser was used as a polymerization source and 785 nm as a Raman probe beam. During consumption of the monomers, the C═C double bond present in the monomer structure is converted into a C–C single bond leading to a decrease of the intensity of the associated Raman peak. Relative polymerization rates were compared by monitoring the decrease in the intensity of these two characteristic acrylamide Raman peaks as a function of 532 nm irradiation time. The peak area ratio was used in order to negate the effect of fluctuations in intensity due to background, scatter, and laser focus.[55b] The peaks at 1600 cm⁻¹ and 1623 cm⁻¹ were each fitted using a Gaussian–Lorentzian function, and the ratio of the peak areas was plotted *versus* time (Fig. 6(c)). The experimental setup and results are shown in more detail in Section S9.3 of the ESI† (Fig. S18 and S19). The results demonstrate that photopolymerization in these materials can be driven under 532 nm irradiation, and that both pyrene and anthracene dyads exhibited comparable photopolymerization rates relative to **BDPI₂** (Fig. S20, ESI†).

Fig. 7(a) represents the real-time diffraction efficiency growth curves of the transmission gratings with the spatial frequency of 800 lines per mm recorded in the layers containing pyrene and anthracene dyads, and reference photosensitizer **BDPI₂** as described in Section S10 of the ESI.† Thickness of the gratings has been estimated from the Bragg selectivity curves (Fig. 7(b) and (c)). Video in the ESI† demonstrates the performance of the transmission gratings recorded in CA–PEG layer sensitized with pyrene dyads under illumination with ambient light. The gratings selectively diffract light with different wavelengths of the spectrum at the specific angles (the Bragg angle).

We attempted to perform holographic patterning of CA–PEG layer containing **BDP 1a** and NPG. After exposure to the total recording intensity of 74 mW cm⁻² for 100 s, no diffracted intensity was detected, and no diffracted beam was observed. This indicates that **BDP 1a** – NPG system has too low free radical generation capability to cause polymerization of acrylamide monomers. This can be explained by inefficient ISC in **BDP 1a** which is manifested by low singlet oxygen generation quantum yields measured for this compound (Table 2).

The photosensitivity of the holographic recording material is directly linked to the polymerization rate, which depends on
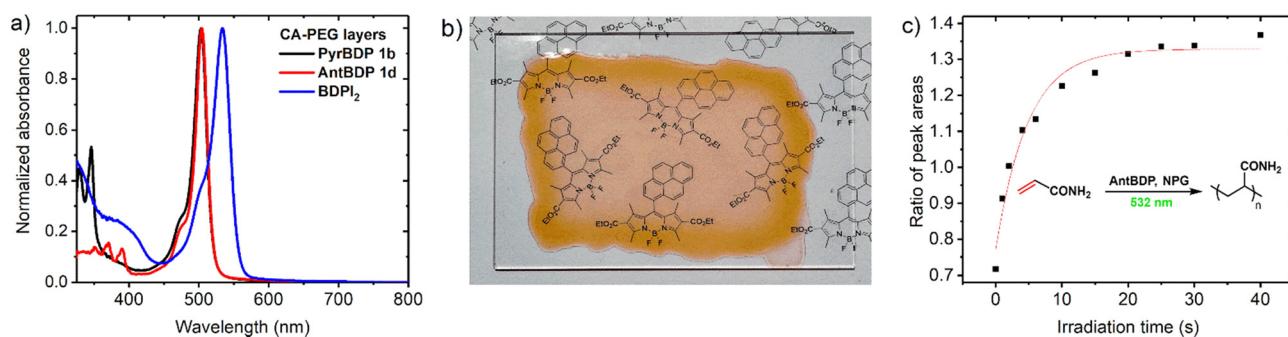
Fig. 6 (a) UV-Vis absorption spectra of layers containing **PyrBDP 1b**, **AntBDP 1d**, and **BDPI₂** as photosensitizers; (b) photograph of a sample of CA–PEG layers containing **PyrBDP 1b** on a glass substrate; (c) graph of ratio between Raman scattering peaks for monomers C═C bonds at ≈1600 and ≈1623 cm⁻¹ *vs.* irradiation time for CA–PEG layer containing **AntBDP 1d**. The sample was exposed to 532 nm light source (10 mW cm⁻²). The red solid line is a mono-exponential growth fitting curve.

This journal is © The Royal Society of Chemistry 2023

J. Mater. Chem. C, 2023, **11**, 15084–15096 | **15091**

Fig. 7 (a) Real time diffraction efficiency evolution for transmission gratings recorded on CA–PEG layers sensitized with dyads **PyrBDP 1b** (74 μm), **AntBDP 1d** (87 μm) and **BDPI₂** (104 μm). The total recording intensity is 20 mW cm^{-2}; (b)–(d) typical Bragg selectivity curves of transm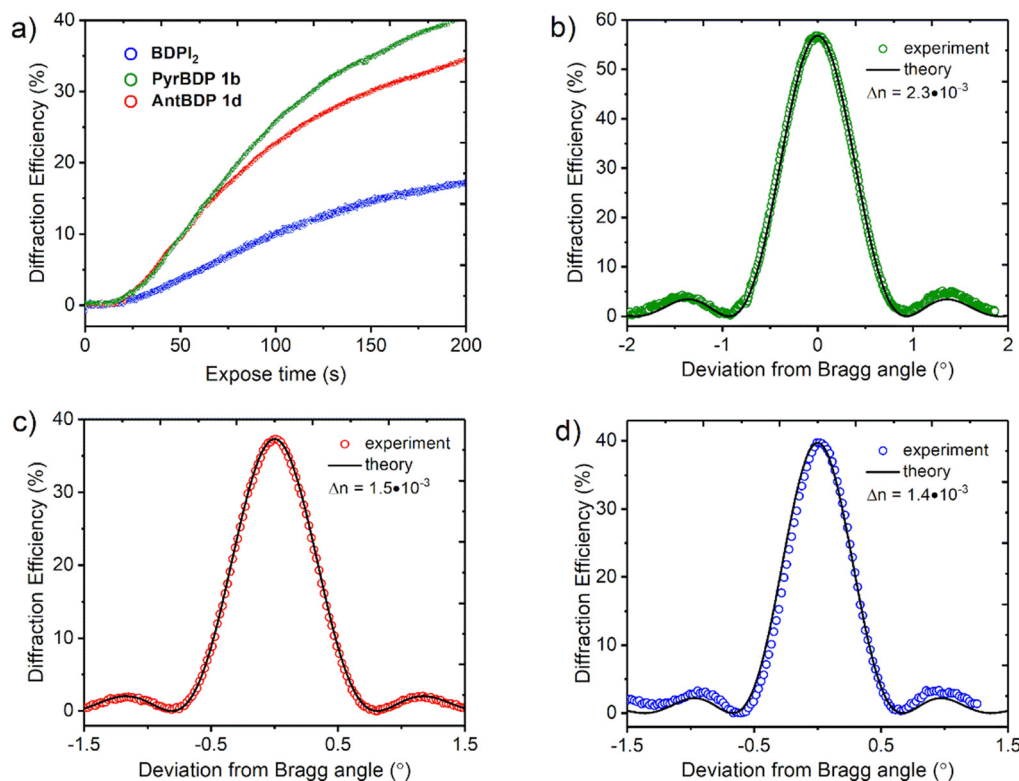ission gratings recorded on CA–PEG layers sensitized with **PyrBDP 1b**, **AntBDP 1d** and **BDPI₂**, respectively. Experimental data are fitted by means of coupled-wave theory (eqn (S5)–(S9), ESI†).

the ability of the photoinitiator to generate free radicals which lead to the formation of polymer chains and, as a result, the diffraction efficiency increase. The photosensitivity has been estimated from the linear part of growth curves (ESI,† Section S10.3). As seen from Fig. 7(a), the linear part of the curves for **PyrBDP 1b** and **AntBDP 1d** have identical slopes, which denotes equal exposure sensitivity of the two compositions, and it is found to be 4×10^{-4} mJ^{-1} cm^2. The slope of the **BDPI₂** curve is lower and corresponds to the exposure sensitivity of 2×10^{-4} mJ^{-1} cm^2. The lower photosensitivity of layers containing **BDPI₂** can be explained by lower efficiency of the photoinitiating system containing **BDPI₂** and NPG to generate free radicals that initiate the formation of polymer chains. Thus, donor–acceptor dyads **PyrBDP 1b** and **AntBDP 1d** have demonstrated a higher capability to initiate free radical polymerization in CA–PEG photopolymer than the reference heavy-atom containing photosensitizer.

Fig. 7(b)–(d) represents typical Bragg selectivity curves of the transmission gratings recorded on layers containing **PyrBDP 1b**, **AntBDP 1d** and **BDPI₂** using an exposure energy of 4 J cm^{-2}. Shelf-life study has showed unchanged diffraction efficiency for all samples for 4 months (see Section S10.4 of the ESI† for details). Further shelf-life study is in progress. Refractive index modulation has been estimated by eqn (S5) (ESI†) and it has been found to be 2.3×10^{-3}, 1.5×10^{-3} and 1.4×10^{-3} for **PyrBDP 1b** (74 μm thick layer), **AntBDP 1d** (87 μm thick layer) and **BDPI₂** (104 μm thick layer), respectively. The obtained

refractive index modulation is comparable to what was achieved in CA–PEG sensitized with Erythrosine B and NPG as reported in our previous work,[18] and in polyvinyl alcohol-based photopolymers sensitized with methylene blue[58] and Erythrosine B[21] (Table 3).

The grating formation mechanism and creation of the refractive index modulation during holographic recording is discussed in the following section.

Grating formation mechanism

In photopolymerizable materials, grating formation mechanism depends on the material composition and the permeability of the matrix which influence the diffusion of mobile species and the resultant refractive index modulation.[56] In volume gratings, the refractive index modulation (Δn) is created by the impact of three mechanisms such as change in density, molar refraction and monomer concentration gradient driven diffusion as described in details further.[57] Firstly, in bright fringe areas (illuminated areas) the density increases due to polymerization, and it has the minimum value in dark fringe areas (not illuminated areas). This leads to different refractive indexes in bright and dark areas, $n_{density}^{bright}$ and $n_{density}^{dark}$, respectively, according to the distribution of the light intensity (Fig. 8(a)–(c)). Secondly, the different degree of polymerization in bright and dark areas causes variation in polarizability due different degree of monomers' C=C bonds conversion which is shifted with respect to the modulation due to density variation

15092 | *J. Mater. Chem. C*, 2023, **11**, 15084–15096

This journal is © The Royal Society of Chemistry 2023

Table 3 Refractive index modulation achieved for reference photopolymers

Refractive index modulation ($\times 10^{-3}$)				
Thickness (μm)	PVA/AA/MB[58]	PVA/NIPA/ErB[21]	Cellulose/AA/ErB[18]	This work
70	1.4	2.4	2.3	2.3 (**PyrBDP 1b**)
85	N/A	2.1	N/A	1.5 (**AntBPD 1d**)
100	N/A	1.8	1.1	1.4 (**BDPI$_2$**)

PVA – polyvinyl alcohol; AA – acrylamide; MB – methylene blue; NIPA – *N*-isopropyl acrylamide; ErB – erythrosine B. N/A – not described.
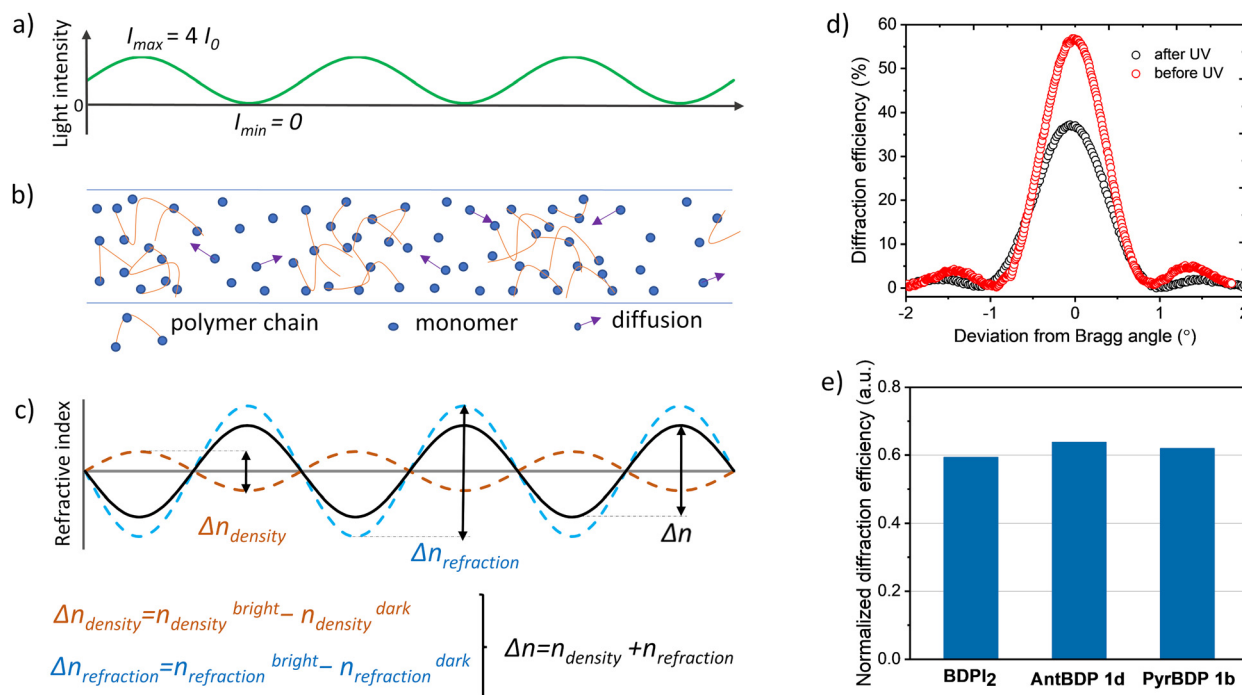
Fig. 8 (a) Spatial variation of the recording light intensity created by two recording beams (with I_0 intensity) during holographic exposure using the set-up shown in Fig. S21 (ESI†); (b) distribution of monomers/polymer chains in the volume of the photopolymerizable material after holographic exposure. Arrows show the diffusion of monomers due to the concentration gradient created by holographic exposure; (c) mechanism of obtaining refractive index modulation in the photopolymerizable material with low diffusion (monomer molecules diffuse slowly and only a small fraction of them reach the bright fringe area); (d) typical Bragg selectivity curves of **PyrBDP 1b** sample measured before and after exposure to uniform UV irradiation; (e) normalised diffraction efficiency shows the change in the diffraction efficiency of transmission gratings recorded in cellulose-PEG layers sensitized with **BDPI$_2$**, **PyrBDP 1b** and **AntBDP 1d** after UV exposure.

by 180°. This provides variation in molar refraction and, as a result, in the refractive index too, such as $\Delta n_{\text{refraction}} = n_{\text{refraction}}^{\text{bright}} - n_{\text{refraction}}^{\text{dark}}$ (Fig. 8(c)). Thirdly, the concentration gradient that occurs during recording leads to the diffusion of monomers. If the diffusion is high then most of the monomers manage to reach bright areas, and the density variation is the main contributor to the refractive index modulation. In case of low diffusion, only a small fraction of monomer molecules reaches the bright area, and structural changes in the monomer molecules play a major role in the formation of refractive index modulation.

Here, we present preliminary results on the grating formation mechanism in CA–PEG sensitized with new BODIPYs and reference **BDPI$_2$**. Our approach is based on the evaluation of the main contributor to the grating formation by applying UV-post exposure with uniform intensity as was previously demonstrated for the acrylamide-based photopolymer containing

Erythrosine B and NPG as photoinitiators.[58] UV post-exposure (after holographic recording) induces changes in the refractive index modulation due to further bond conversion evenly through the thickness. Changes in the refractive index modulation can be estimated by evaluating the changes in the diffraction efficiency as these parameters are correlated according to the coupled wave theory as described in Section S10.2 of the (ESI†).[59]

Gratings recorded on 80 ± 5 μm thick layers (**PyrBDP 1b**, **AntBDP 1d** and **BDPI$_2$**) using the exposure energy of 4 J cm^{-2} were exposed to UVA light with a Dymax UV-curing System (ECE Series). During UV exposure, an energy of 26.3 J cm^{-2} was used and the diffraction efficiency was measured before and after UV exposure. The normalized diffraction efficiency was calculated as their ratio. Typical Bragg selectivity curves before and after UV-exposure are presented in Fig. 8(d). As seen from Fig. 8(e), the diffraction efficiency of **PyrBDP 1b**, **AntBDP 1d** and **BDPI$_2$**

This journal is © The Royal Society of Chemistry 2023

J. Mater. Chem. C, 2023, **11**, 15084–15096 | **15093**

decreases to 38, 36 and 40.6%, respectively, after UV exposure. The observed decrease of the refractive index modulation indicates that the bond conversion is the main contributor to the grating formation which assumes that the matrix has low permeability and that the mobile species' diffusion is restricted.[58] Further investigation of the photopolymerization kinetics, relationship between the rate of polymerization and the concentrations of monomer, polymer, dye, and initiator is required in order to develop the model of the grating formation mechanism in CA–PEG sensitized with the studied BODIPY dyes. The model will allow to predict the material response at different special frequencies and achieve its full potential. This will be the focus of our future work.

Conclusion

In this work, we designed and synthesized a series of novel heavy-atom-free SOCT-ISC photosensitizers based on 2,6-diethoxycarbonyl-BODIPY scaffold as an electron acceptor. Due to increased electron acceptor ability of this BODIPY scaffold, dyads with pyrene and anthracene groups as electron donors undergo efficient charge transfer and triplets' formation in non-polar solvent, such as toluene, which is desired for application of these dyes as photoinitiators for polymerization. Transient absorption spectroscopy data confirmed that intramolecular charge separation takes place on a picosecond time-scale, followed by recombination of CT states into triplet excited states of BODIPY *via* SOCT-ISC. For the lead BODIPY-anthracene compound **1c**, excellent photosensitization ability was observed as is evidenced by singlet oxygen generation quantum yields of up to 94%.

In combination with NPG as a co-initiator, diethoxycarbonyl-BODIPY have showed the ability to initiate free-radical polymerization of acrylamide monomers under 532 nm irradiation, allowing for the formation of volume transmission gratings in a cellulose acetate-based photopolymer. The novel heavy-atom-free photosensitizers provide higher exposure sensitivity than a reference heavy-atom-containing dye, **BDPI$_2$**. High diffraction efficiency (up to 56%) was obtained for CA–PEG layers sensitized with pyrene and anthracene dyads, proving that they can efficiently operate as a photosensitizers and initiate recording of diffractive structures. The developed photopolymerizable material showed high refractive index modulation (up to 2.3 $\times 10^{-3}$), low scattering, and good mechanical and chemical stability. In addition, unchanged diffraction efficiency was observed for 4 months after the recording. These results provide further perspective for the utilisation of heavy-atom-free BODIPYs as components of photoinitiating systems and expand the arsenal of environment-friendly and sustainable photopolymerizable materials for holography.

Author contributions

A. S. and M. F. synthesized new dyes, studied steady-state optical properties and singlet oxygen generation, prepared CA–PEG layers and performed photopolymerization tests using Raman spectroscopy. T. M. and I. N. performed holographic recording experiments and interpreted the results. C. D. C., S. K., W. A. and F. L. performed spectroscopic measurements and interpreted the results. M. D. assisted in synthesis and characterization of new compounds. S. G. and I. N. developed the procedure for CA–PEG layers preparation and assisted in synthesis of materials. H. J. B. assisted with interpretation of Raman spectroscopy data. A. S., T. M., C. D. C., and M. F. wrote the manuscript. M. F. conceived the idea of this study and supervised the project.

Conflicts of interest

There are no conflicts to declare.

Acknowledgements

References

1 J. Shao, Y. Huang and Q. Fan, *Polym. Chem.*, 2014, **5**, 4195–4210.

2 (*a*) P. Chittavanich, K. Miller and M. D. Soucek, *Prog. Org. Coatings*, 2012, **73**, 392–400; (*b*) N. Corrigan, J. Yeow, P. Judzewitsch, J. Xu and C. Boyer, *Angew. Chem., Int. Ed.*, 2019, **58**, 5170–5189.

3 P. Lederhose, Z. Chen, R. Müller, J. P. Blinco, S. Wu and C. Barner-Kowollik, *Angew. Chem., Int. Ed.*, 2016, **55**, 12195–12199.

4 A. Balcerak and J. Kabatc, *Polym. Chem.*, 2022, **13**, 1787–1812.

5 D. Sasikumar, A. T. John, J. Sunny and M. Hariharan, *Chem. Soc. Rev.*, 2020, **49**, 6122–6140.

6 J. Zhao, W. Wu, J. Suna and S. Guo, *Chem. Soc. Rev.*, 2013, **42**, 5323.

7 X. Zhang, Z. Wang, Y. Hou, Y. Yan, J. Zhao and B. Dick, *J. Mater. Chem. C*, 2021, **9**, 11944–11973.

8 (*a*) S. Callaghan, M. A. Filatov, H. Savoie, R. W. Boyle and M. O. Senge, *Photochem. Photobiol. Sci.*, 2019, **18**, 495–504; (*b*) J. Deckers, T. Cardeynaels, H. Penxten, A. Ethirajan, M. Ameloot, M. Kruk, B. Champagne and W. Maes, *Chem. – Eur. J.*, 2020, **26**, 15212–15225; (*c*) J. Jiménez, R. Prieto-Montero, B. L. Maroto, F. Moreno, M. J. Ortiz, A. Oliden-Sánchez, I. López-Arbeloa, V. Martínez-Martínez and S. de la Moya, *Chem. – Eur. J.*, 2020, **26**, 601–605; (*d*) V.-N. Nguyen, Y. Yan, J. Zhao and J. Yoon, *Acc. Chem. Res.*, 2021, **54**, 207–220; (*e*) R. Prieto-Montero, A. D. Andres, A. Prieto-Castañeda, A. Tabero, A. Longarte, A. R. Agarrabeitia,

15094 | *J. Mater. Chem. C*, 2023, **11**, 15084–15096

This journal is © The Royal Society of Chemistry 2023

A. Villanueva, M. J. Ortiz, R. Montero, D. Casanova and V. Martínez-Martínez, *J. Mater. Chem. B*, 2023, **11**, 169–179.

9 (a) N. Kiseleva, M. A. Filatov, M. Oldenburg, D. Busko, M. Jakoby, I. A. Howard, B. S. Richards, M. O. Senge, S. M. Borisov and A. Turshatov, *Chem. Commun.*, 2018, **54**, 1607–1610; (b) Y. Dong, A. A. Sukhanov, J. Zhao, A. Elmali, X. Li, B. Dick, A. Karatay and V. K. Voronkova, *J. Phys. Chem. C*, 2019, **123**, 22793–22811; (c) Y. Hu, Y. Hou, Z. Wang, Y. Li and J. Zhao, *J. Chem. Phys.*, 2020, **153**, 224304; (d) N. Kiseleva, D. Busko, B. S. Richards, M. A. Filatov and A. Turshatov, *J. Phys. Chem. Lett.*, 2020, **11**, 6560–6566; (e) R. A. Arellano-Reyes, A. Prabhakaran, R. C. E. Sia, J. Guthmuller, K. K. Jha, T. Yang, B. Dietzek-Ivanšić, V. McKee and T. E. Keyes, *Chem. – Eur. J.*, 2023, **29**, e202300239.

10 H. Lu, J. Mack, Y. Yang and Z. Shen, *Chem. Soc. Rev.*, 2014, **43**, 4778–4823.

11 (a) M. A. Filatov, *Org. Biomol. Chem.*, 2020, **18**, 10–27; (b) E. Bassan, A. Gualandi, P. G. Cozzi and P. Ceroni, *Chem. Sci.*, 2021, **12**, 6607–6628.

12 T. Mikulchyk, S. Karuthedath, C. S. P. De Castro, A. A. Buglak, A. Sheehan, A. Wieder, F. Laquai, I. Naydenova and M. A. Filatov, *J. Mater. Chem. C*, 2022, **10**, 11588–11597.

13 F. Dumur, *Eur. Polym. J.*, 2023, **196**, 112241.

14 A. Uddin, S. R. Allen, A. K. Rylski, C. J. O'Dea, J. T. Ly, T. A. Grusenmeyer, S. T. Roberts and Z. A. Page, *Angew. Chem., Int. Ed.*, 2023, **62**, e202219140.

15 M. Topa, F. Petko, M. Galek, K. Machowski, M. Pilch, P. Szymaszek and J. Ortyl, *Polymers*, 2019, **11**, 1756.

16 J. T. Buck, A. M. Boudreau, A. DeCarmine, R. W. Wilson, J. Hampsey and T. Mani, *Chem*, 2018, **5**, 1.

17 A. A. Buglak, A. Charisiadis, A. Sheehan, C. J. Kingsbury, M. O. Senge and M. A. Filatov, *Chem. – Eur. J.*, 2021, **27**, 9934–9947.

18 S.-e.- Gul, J. Cassidy and I. Naydenova, *Photonics*, 2021, **8**, 329.

19 J. Zhang, J. Lalevée, X. Mou, F. Morlet-Savary, B. Graff and P. Xiao, *Macromolecules*, 2018, **51**, 3767.

20 A. Al Mousawi, P. Garra, M. Schmitt, J. Toufaily, T. Hamieh, B. Graff, J. P. Fouassier, F. Dumur and J. Lalevée, *Macromolecules*, 2018, **51**, 4633.

21 T. Mikulchyk, S. Martin and I. Naydenova, *Appl. Opt.*, 2017, **56**, 6348.

22 Q. Gong, S. Wang, M. Huang and F. Gan, *Mater. Lett.*, 2005, **59**, 2969.

23 G. Qiaoxia, H. Mingju and G. Fuxi, *Dyes Pigm.*, 2006, **69**, 204.

24 S. Ikeda, S. Murata, K. Ishii and H. Hamaguchi, *Chem. Lett.*, 1999, 1009.

25 (a) R. Malallah, H. Li, D. Kelly, J. Healy and J. Sheridan, *Polymers*, 2017, **9**, 337; (b) F.-K. Bruder, R. Hagen, T. Rölle, M.-S. Weiser and T. Faecke, *Angew. Chem., Int. Ed.*, 2011, **50**, 4552.

26 G. A. Cordell, *J. Org. Chem.*, 1975, **40**, 3161–3169.

27 A. Treibs and F.-H. Kreuzer, *Justus Liebigs Ann. Chem.*, 1968, **718**, 208–223.

28 (a) H. Falk and G. Schoppel, *Monatsh. Chem.*, 1990, **121**, 67–76; (b) N. O. Didukh, V. P. Yakubovskyi, Y. V. Zatsikha, V. N. Nemykin and Y. P. Kovtun, *Dyes Pigm.*, 2018, **149**, 774–782; (c) N. O. Didukh, V. P. Yakubovskyi, Y. V. Zatsikha, G. T. Rohde, V. N. Nemykin and Y. P. Kovtun, *J. Org. Chem.*, 2019, **84**, 2133–2147.

29 A. Loudet and K. Burgess, *Chem. Rev.*, 2007, **107**, 4891–4932.

30 Y. Gabe, Y. Urano, K. Kikuchi, H. Kojima and T. Nagano, *J. Am. Chem. Soc.*, 2004, **126**, 3357–3367.

31 J.-J. Shie, Y.-C. Liu, Y.-M. Lee, C. Lim, J.-M. Fang and C.-H. Wong, *J. Am. Chem. Soc.*, 2014, **136**, 9953–9961.

32 A. B. Descalzo, P. Ashokkumar, Z. Shen and K. Rurack, *ChemPhotoChem*, 2020, **4**, 120–131.

33 (a) M. A. Filatov, S. Karuthedath, P. M. Polestshuk, S. Callaghan, K. J. Flanagan, T. Wiesner, F. Laquai and M. O. Senge, *ChemPhotoChem*, 2018, **2**, 606–615; (b) N. Kiseleva, M. A. Filatov, J. C. Fischer, M. Kaiser, M. Jakoby, D. Busko, I. A. Howard, B. S. Richards and A. Turshatov, *Phys. Chem. Chem. Phys.*, 2022, **24**, 3568.

34 D. P. Kennedy, C. M. Kormos and S. C. Burdette, *J. Am. Chem. Soc.*, 2009, **131**, 8578–8586.

35 E. S. Pysh and N. C. Yang, *J. Am. Chem. Soc.*, 1963, **85**, 2124–2130.

36 R. F. Kubin and A. N. Fletcher, *J. Lumin.*, 1982, **27**, 455–462.

37 (a) M. A. Filatov, S. Karuthedath, P. M. Polestshuk, H. Savoie, K. J. Flanagan, C. Sy, E. Sitte, M. Telitchko, F. Laquai, R. W. Boyle and M. O. Senge, *J. Am. Chem. Soc.*, 2017, **139**, 6282; (b) M. A. Filatov, S. Karuthedath, P. M. Polestshuk, S. Callaghan, K. J. Flanagan, M. Telitchko, T. Wiesner, F. Laquai and M. O. Senge, *Phys. Chem. Chem. Phys.*, 2018, **20**, 8016–8031.

38 P. Luo, E. C. Feinberg, G. Guirado, S. Farid and J. P. Dinnocenzo, *J. Org. Chem.*, 2014, **79**, 9297–9304.

39 (a) Z. E. X. Dance, S. M. Mickley, T. M. Wilson, A. B. Ricks, A. M. Scott, M. A. Ratner and M. R. Wasielewski, *J. Phys. Chem. A*, 2008, **112**, 4194; (b) Z. E. X. Dance, Q. Mi, D. W. McCamant, M. J. Ahrens, M. A. Ratner and M. R. Wasielewski, *J. Phys. Chem. B*, 2006, **110**, 25163.

40 E. Gross, B. Ehrenberg and F. M. Johnson, *Photochem. Photobiol.*, 1993, **57**, 808.

41 Y. Zhao, R. Duan, J. Zhao and C. Li, *Chem. Commun.*, 2018, **54**, 12329–12332.

42 B. Lang, S. Mosquera-Vázquez, D. Lovy, P. Sherin, V. Markovic and E. Vauthey, *Rev. Sci. Instrum.*, 2013, **84**, 73107.

43 P. Foggi, L. Pettini, I. Santa, R. Righini and S. Califano, *J. Phys. Chem.*, 1995, **99**, 7439–7445.

44 L. Ludvíková, P. Friš, D. Heger, P. Šebej, J. Wirza and P. Klán, *Phys. Chem. Chem. Phys.*, 2016, **18**, 16266–16273.

45 S. Vyas, P.-H. Wang and Y. Luo, *Opt. Express*, 2017, **25**, 23726.

46 P. Hu, J. Li, J. Jin, X. Lin and X. Tan, *ACS Appl. Mater. Interfaces*, 2022, **14**, 21544–21554.

47 N. Vorzobova and P. Sokolov, *Polymers*, 2019, **11**, 2020.

48 (a) Z. Shen, Y. Weng, Y. Zhang, C. Wang, A. Liu and X. Li, *Polymers*, 2021, **13**, 936; (b) J. Xiong, K. Yin, K. Li and S.-T. Wu, *Adv. Photonics Res.*, 2021, **2**, 2000049; (c) X. Duan, J. Liu, X. Shi, Z. Zhang and J. Xiao, *Opt. Express*, 2020, **28**, 31316; (d) M. V. Shishova, S. B. Odinokov,

This journal is © The Royal Society of Chemistry 2023

J. Mater. Chem. C, 2023, **11**, 15084–15096 | **15095**

A. Y. Zherdev and D. S. Lushnikov, *Appl. Opt.*, 2021, **60**, A140–A144; (*e*) C. Jang, C. Lee, J. Jeong, G. Li, S. Lee, J. Yeom, K. Hong and B. Lee, *Appl. Opt.*, 2016, **55**, A71–A85; (*f*) J. Xiong, K. Yin, K. Li and S.-T. Wu, *Adv. Photonics Res.*, 2021, **2**, 2000049.

49 M. R. Gleeson, J. V. Kelly, D. Sabol, C. E. Close, S. Liu and J. T. Sheridan, *J. Appl. Phys.*, 2007, **102**, 023108.

50 A. Ibrahim, X. Allonas, C. Ley, K. Kawamura, H. Berneth, F.-K. Bruder, T. Fäcke, R. Hagen, D. Hönel, T. Rölle, G. Walze and M. S. Weiser, *Chem. – Eur. J.*, 2014, **20**, 15102–15107.

51 Y. Liu, T. Shen, B. Kang, S. Li, Z. Zheng, H. Lv and J. Zheng, *Opt. Laser Technol.*, 2022, **156**, 108580.

52 H. Berneth, F. K. Bruder, T. Fäcke, S. Hansen, K. Kawamura, L. Pitzer, S. Kern, B. Wewer and T. A. Rölle, *Polymers*, 2021, **13**, 3517.

53 A. Narita, J. Oshima, Y. Iso, S. Hasegawa and Y. Tomita, *Opt. Mater. Express*, 2021, **11**, 614–628.

54 J. M. Aubry, C. Pierlot, J. Rigaudy and R. Schmidt, *Acc. Chem. Res.*, 2003, **36**, 668.

55 (*a*) R. Jallapuram, I. Naydenova, H. J. Byrne, S. Martin, R. Howard and V. Toal, *Appl. Opt.*, 2008, **47**, 206; (*b*) D. Cody, E. Mihaylova, L. O'Neill and I. Naydenova, *Opt. Mater.*, 2015, **48**, 12–17.

56 S. Blaya, L. Carretero, R. F. Madrigal, M. Ulibarrena, P. Acebal and A. Fimia, *Appl. Phys. B*, 2003, **77**, 639–662.

57 E. S. Gyulnazarov, T. N. Smirnova and E. A. Tikhonov, *Opt. Spectrosc.*, 1989, **67**, 99.

58 T. Mikulchyk, S. Martin and I. Naydenova, *Opt. Mater.*, 2014, **37**, 810–815.

59 H. Kogelnik, *Bell Syst. Tech. J.*, 1969, **48**, 2909–2947.

15096 | *J. Mater. Chem. C*, 2023, **11**, 15084–15096

This journal is © The Royal Society of Chemistry 2023